SUPPORTING INFORMATION

Near Length-Independent Conductance in Polymethine Molecular Wires

Suman Gunasekaran,[1] Daniel Hernangómez-Pérez,[2] Iryna Davydenko,[3] Seth Marder,[3*] Ferdinand Evers,[2*] Latha Venkataraman[1,4*]

[1]Department of Chemistry, Columbia University, New York, New York 10027, United States
[2]Institute of Theoretical Physics, University of Regensburg, 93040 Regensburg, Germany
[3]School of Chemistry and Biochemistry and Center for Organic Photonics and Electronics, Georgia Institute of Technology, Atlanta, Georgia 30332-0400, United States
[4]Department of Applied Physics and Applied Mathematics, Columbia University, New York, New York 10027, United States

*E-mail: seth.marder@chemistry.gatech.edu, ferdinand.evers@physik.uni-regensburg.de, lv2117@columbia.edu (Phone: 212-854-1786)

Contents:

1. Synthetic Details

Trimethine cyanine **D1** (**ID-III-73**), pentamethine cyanine **D2** (**ID-III-71**) and heptamethine cyanine **D3** (**ID-III-69**) were prepared using standard procedures. Commercially available intermediates were purchased and used without further purification. ^{1}H and $^{13}C\{^{1}H\}$ NMR spectra were recorded on a Bruker Avance IIIHD 500 instrument operating at 500 MHz, 125 MHz respectively. Mass spectra were measured on a VG Instruments 70-SE using the electron impact (EI). Elemental analyses were carried out by Atlantic Microlab using a LECO 932 CHNS elemental analyzer.

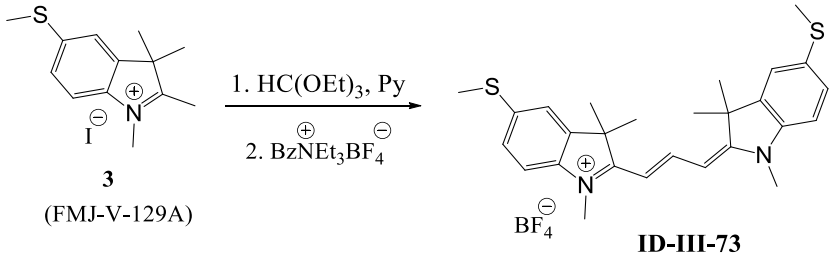

3 (FMJ-V-129A)

ID-III-73

Synthesis of **D1** (**ID-III-73**). A solution of quaternary salt **3** (0.104 g, 0.3 mmol, 2 eq.) and 0.1 mL of triethyl orthoformate (cas 122-51-0) in pyridine (3 mL) was heated at 75 ºC (bath temperature) for 15 min under nitrogen. Then solution of benzyltriethylammonium tetrafluoroborate (0.084 g, 0.3 mmol, 2 eq.) in 1 mL of methanol was added to the purple solution and reaction mixture was further heated at 75 ºC (bath temperature) for 10 min. After cooling to room temperature, the diethyl ether (20 mL) was added. The resulting precipitate was filtered off and washed with diethyl ether (3 × 5 mL). The residue was purified by column chromatography on silica gel using methanol:chloroform (3:97 changing to 5:95) as the eluent. The product was purified by recrystallization from 1:4 mixture of acetonitrile and ethanol (5 mL) with benzyltriethylammonium tetrafluoroborate (0.084 g, 0.3 mmol). The dye was dissolved in dichloromethane, followed by filtering the solution and evaporating. Yield 0.035 g, 44 %. ^{1}H NMR (500 MHz, (CD_3CN): δ 8.38 (t, $^{3}J_{HH}$ = 13.5 Hz, 1H), 7.43 (d, $^{3}J_{HH}$ = 2 Hz, 2H), 7.32 (dd, J_1 = 2 Hz, J_2 = 8.5 Hz, 2H), 7.20 (d, $^{3}J_{HH}$ = 8.5 Hz, 2H), 6.24 (d, $^{3}J_{HH}$ = 13.5 Hz, 2H), 3.54 (s, 6H), 2.53 (s, 6H), 1.70 (s, 12H). $^{13}C\{^{1}H\}$ NMR (125 MHz, (CD_3CN): δ 175.16, 150.50, 142.81, 141.76, 136.96, 127.64, 121.70, 112.52, 103.27, 50.26, 32.22, 27.96, 16.45. HRMS (ESI): [M] = 449.2071 (calculated for $C_{27}H_{33}N_2S_2$ 449.2080, ($[M–BF_4]^+$)); ESI^-: [BF_4] = 86.7. Anal. calcd. for $C_{27}H_{33}BF_4N_2S_2\times CH_2Cl_2$: C, 54.12; H, 5.68; N, 4.51. Found: C, 54.40; H, 5.54; N, 4.56.

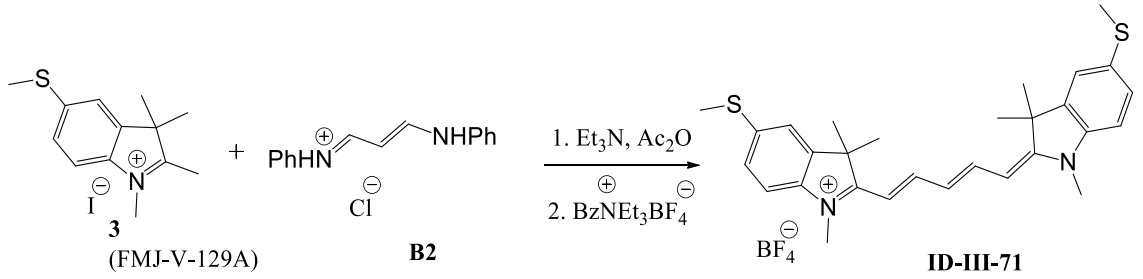

3 (FMJ-V-129A) B2 ID-III-71

Synthesis of **D2** (**ID-III-71**). A solution of quaternary salt **3** (0.104 g, 0.3 mmol, 2 eq.) and malonaldehyde dianilide hydrochloride **B2** (0.039 g, 0.15 mmol, 1 eq.) in acetic anhydride (2 mL), and triethylamine (0.030 g, 0.04 mL, 0.3 mmol, 2 eq.) was heated at 100 ºC (bath temperature) for 25 min under nitrogen. Then benzyltriethylammonium tetrafluoroborate (0.084 g, 0.3 mmol, 2 eq.) was added to the blue solution and reaction mixture was further heated at 100 ºC (bath temperature) for 15 min. After cooling to room temperature, the diethyl ether (10 mL) was added. The resulting precipitate was filtered off and washed with diethyl ether (3 × 5 mL). The residue was purified by column chromatography on silica gel using methanol:dichloromethane (1:99) as the eluent. The product was purified by recrystallization from 1:2 mixture of acetonitrile and ethanol (3 mL) with benzyltriethylammonium tetrafluoroborate (0.084 g, 0.3 mmol). Yield 0.053 g, 63 %. ^{1}H NMR (500 MHz, (CD_3CN): δ 8.03 (t, $^{3}J_{HH}$ = 13 Hz, 2H), 7.40 (d, $^{3}J_{HH}$ = 1.5 Hz, 2H), 7.30 (dd, J_1 = 1.5 Hz, J_2 = 8.5 Hz, 2H), 7.15 (d, $^{3}J_{HH}$ = 8.5 Hz, 2H), 6.50 (t, $^{3}J_{HH}$ = 12.5 Hz, 1H), 6.14 (d, $^{3}J_{HH}$ = 14 Hz, 2H), 3.50 (s, 6H), 2.52 (s, 6H), 1.67 (s, 12H). $^{13}C\{^{1}H\}$ NMR (125 MHz, (CD_3CN): δ 173.90, 154.08, 143.25, 141.96, 136.34, 127.62, 125.44, 121.76, 112.20, 104.02, 50.11, 32.03, 27.50, 16.55. HRMS (ESI): [M] = 475.2229 (calculated for $C_{29}H_{35}N_2S_2$ 475.2236, ($[M–BF_4]^+$)). ; ESI^-: [BF_4] = 86.7. Anal. calcd. for $C_{29}H_{35}BF_4N_2S_2\times H_2O$: C, 60.00; H, 6.42; N, 4.83. Found: C, 59.98; H, 6.46; N, 4.89.

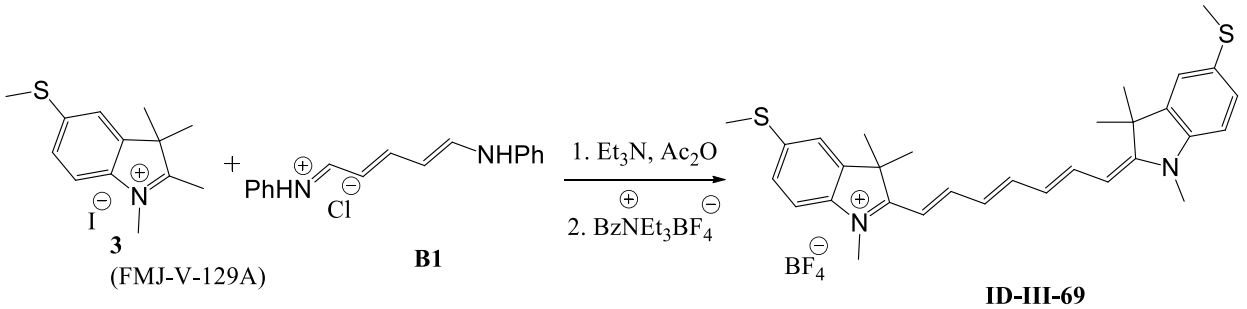

3 (FMJ-V-129A) B1 ID-III-69

Synthesis of **D3** (**ID-III-69**). A solution of quaternary salt **3** (0.104 g, 0.3 mmol, 2 eq.) and *N*-(5-anilino-2,4-pentadienylidene)aniline hydrochloride **B1** (0.043 g, 0.15 mmol, 1 eq.) in acetic

anhydride (2 mL), and triethylamine (0.030 g, 0.04 mL, 0.3 mmol, 2 eq.) was heated at 70 ºC (bath temperature) for 20 min under nitrogen. Then benzyltriethylammonium tetrafluoroborate (0.084 g, 0.3 mmol, 2 eq.) was added to the green solution and reaction mixture was further heated at 70 ºC (bath temperature) for 15 min. After cooling to room temperature, the diethyl ether (15 mL) was added. The resulting precipitate was filtered off and washed with diethyl ether (3 × 5 mL). The residue was purified by column chromatography on silica gel using methanol:dichloromethane (initially 1:99, changing to 3:97) as the eluent. The product was purified by recrystallization from 1:2 mixture of acetonitrile and ethanol (4.5 mL) with benzyltriethyl-ammonium tetrafluoroborate (0.084 g, 0.3 mmol). Yield 0.051 g, 58 %. ^{1}H NMR (500 MHz, (CD_3CN): δ 7.76 (t, $^{3}J_{HH}$ = 13 Hz, 2H), 7.51 (t, $^{3}J_{HH}$ = 13 Hz, 1H), 7.38 (d, $^{3}J_{HH}$ = 1.5 Hz, 2H), 7.28 (dd, J_1 = 1.5 Hz, J_2 = 8 Hz, 2H), 7.13 (d, $^{3}J_{HH}$ = 8 Hz, 2H), 6.47 (t, $^{3}J_{HH}$ = 12.5 Hz, 2H), 6.14 (d, $^{3}J_{HH}$ = 14 Hz, 2H), 3.48 (s, 6H), 2.51 (s, 6H), 1.63 (s, 12H). $^{13}C\{^{1}H\}$ NMR (125 MHz, (CD_3CN): δ 172.46, 156.11 (br.s), 151.34, 143.11, 142.13, 136.07, 127.78, 126.29 (br.s), 121.85, 112.04, 104.68, 49.90, 32.02, 27.61, 16.64. HRMS (ESI): [M] = 501.2385 (calculated for $C_{31}H_{37}N_2S_2$ 501.2393, ($[M–BF_4]^+$)); ESI$^-$: [BF_4] = 86.7. Anal. calcd. for $C_{31}H_{37}BF_4N_2S_2$×0.5 CH_2Cl_2: C, 59.95; H, 6.07; N, 4.44. Found: C, 59.67; H, 6.30; N, 4.38.

2. Cyclic Voltammetry

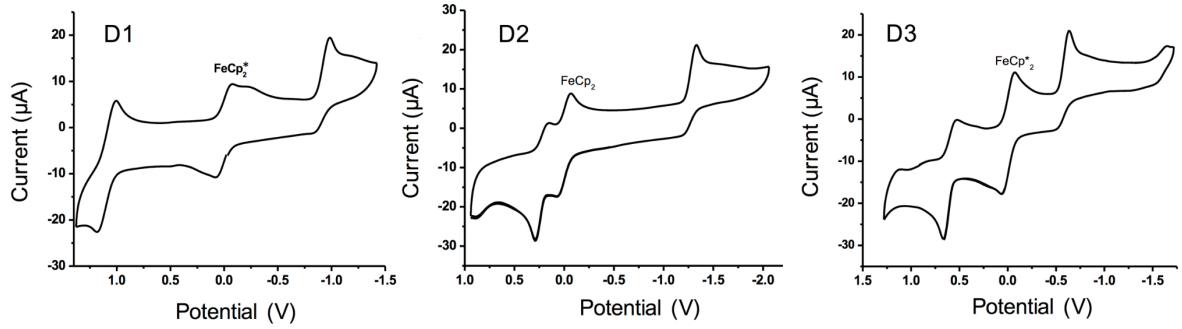

Figure S1. Cyclic voltammograms for cyanines **D1-D3** in CH_2Cl_2/0.1M $NBu_4^+PF6^-$ were recorded at a scan rate of 50 mV s^{-1}. Potentials are plotted vs. ferrocenium / ferrocene ($FeCp_2^+$/$FeCp_2$) for **D2** and decamethyferrocenium/ decamethyl-ferrocene ($FeCp^*_2{}^+$/$FeCp^*_2$) for **D3** and **D1** ($FeCp^*_2$ was determined to be -0.55 V vs. $FeCp_2$ in dichloromethane). The half-wave oxidation potentials converted to the $FeCp_2^+$ for **D1-D3** are: 0.53 V, 0.19 V and 0.04 V. The half-wave reduction potentials converted to the $FeCp_2^+$ for **D1-D3** are: -1.46 V, -1.26 V and -1.13V.

Electrochemical measurements were carried out under an inert atmosphere in dry deoxygenated dichloromethane solution containing 0.1 M tetrabutylammonium hexa-

fluorophosphate as electrolyte. A CH-Instrument 620D potentiostat equipped with a conventional three-electrode cell utilizing a glassy carbon working electrode, platinum wire counter electrode, and a silver wire coated with silver chloride as the pseudo-reference electrode, was used for the measurements.

3. NMR Spectra

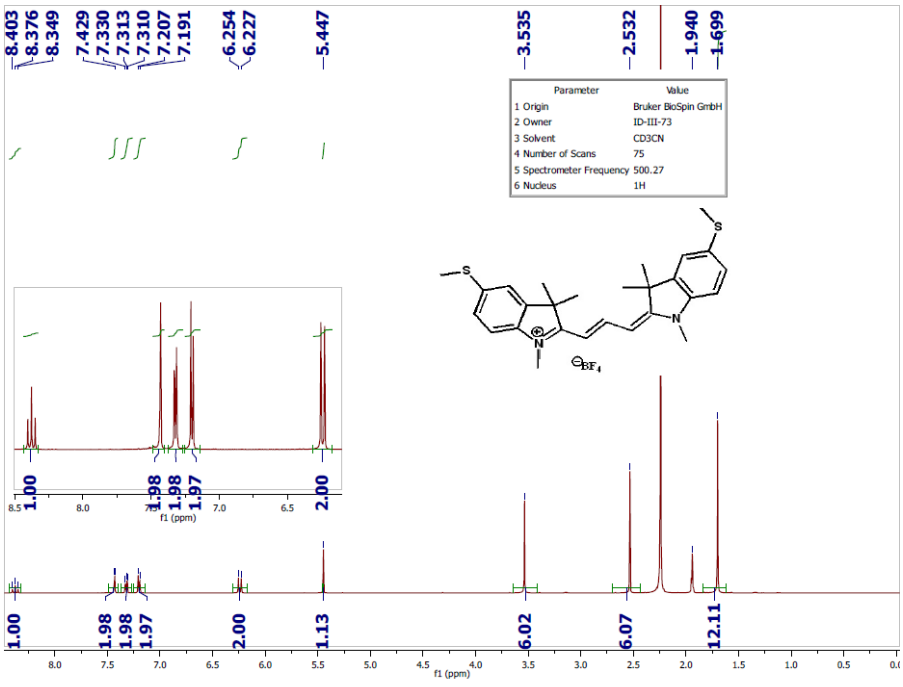

^{1}H NMR for compound **D1** in CD_3CN.

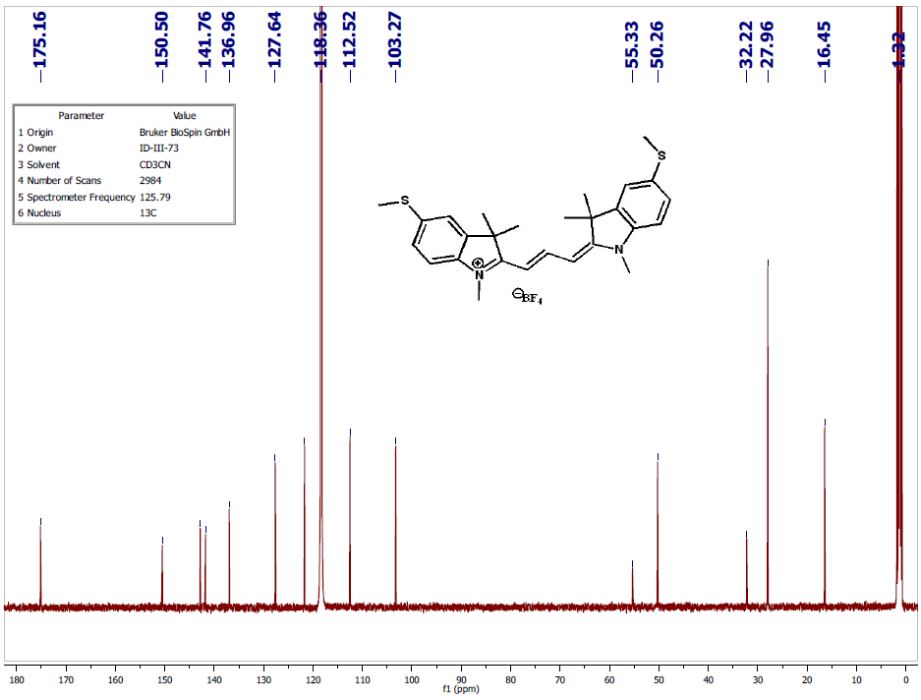

$^{13}C\{^{1}H\}$ NMR for compound **D1** in CD_3CN.

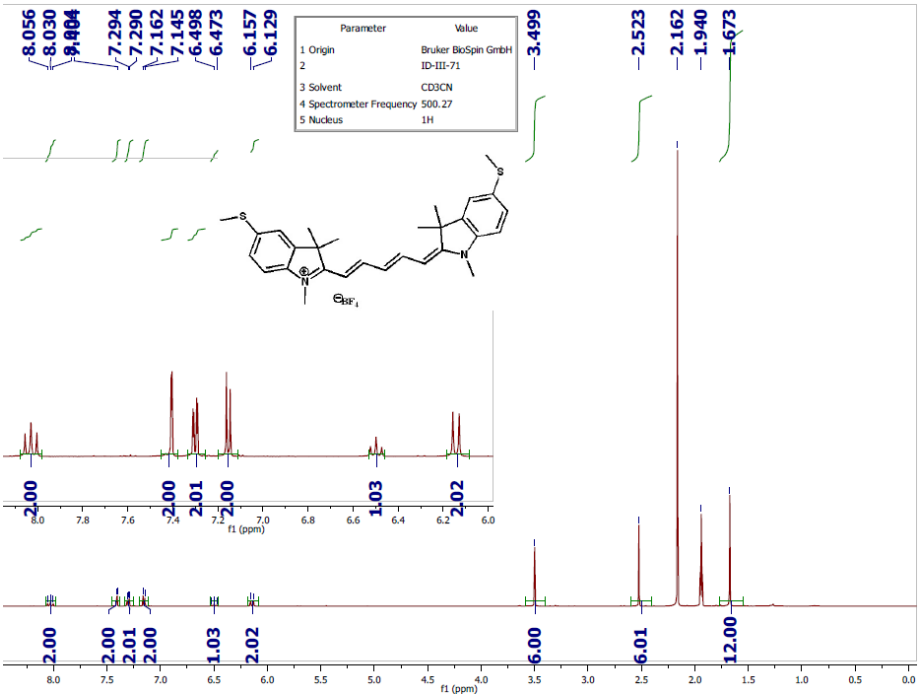

^{1}H NMR for compound **D2** in CD_3CN.

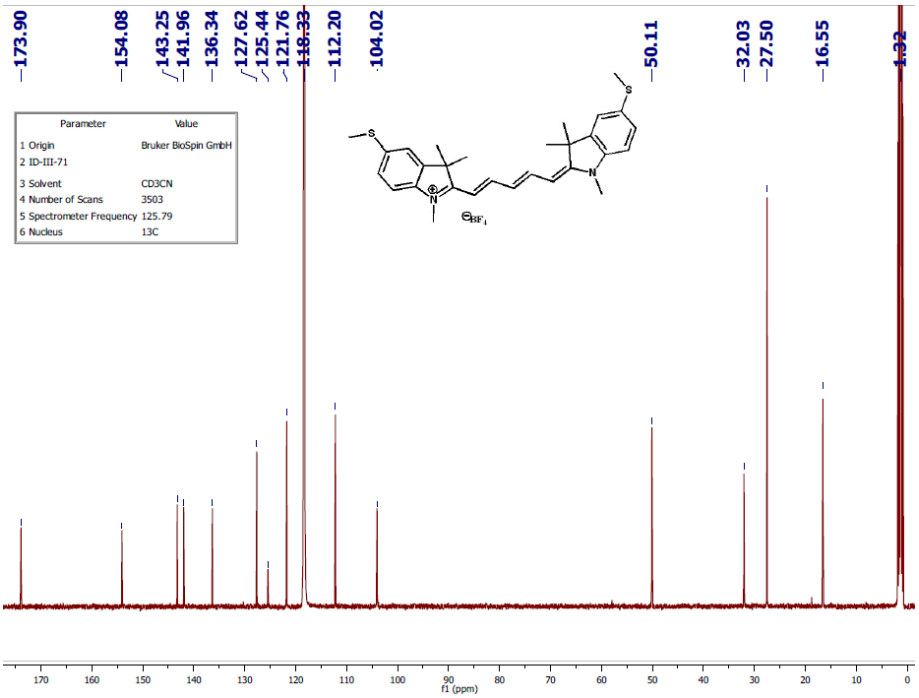

$^{13}C\{^{1}H\}$ NMR for compound **D2** in CD_3CN.

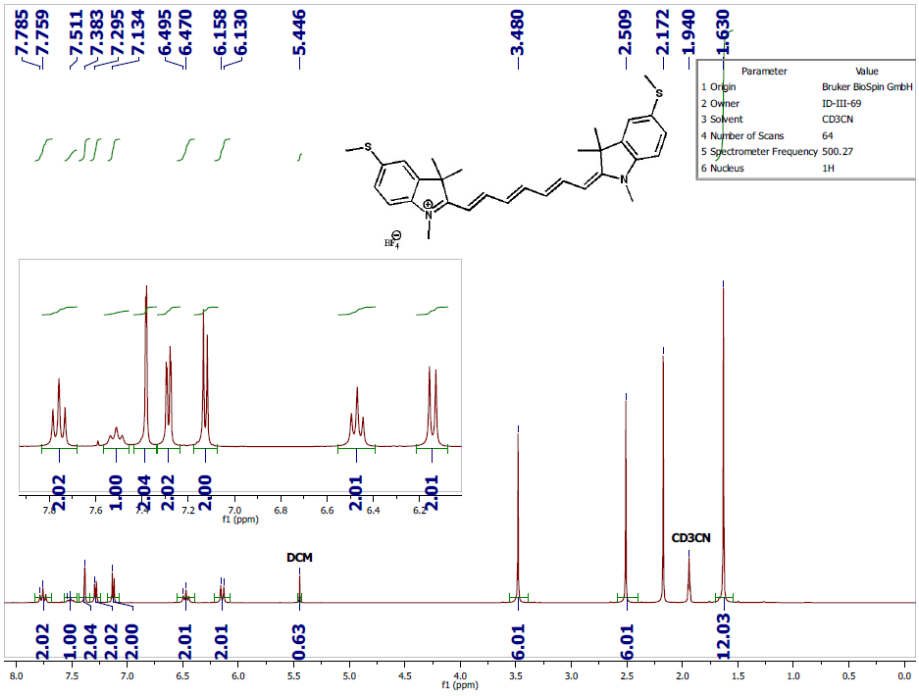

^{1}H NMR for compound **D3** in CD_3CN.

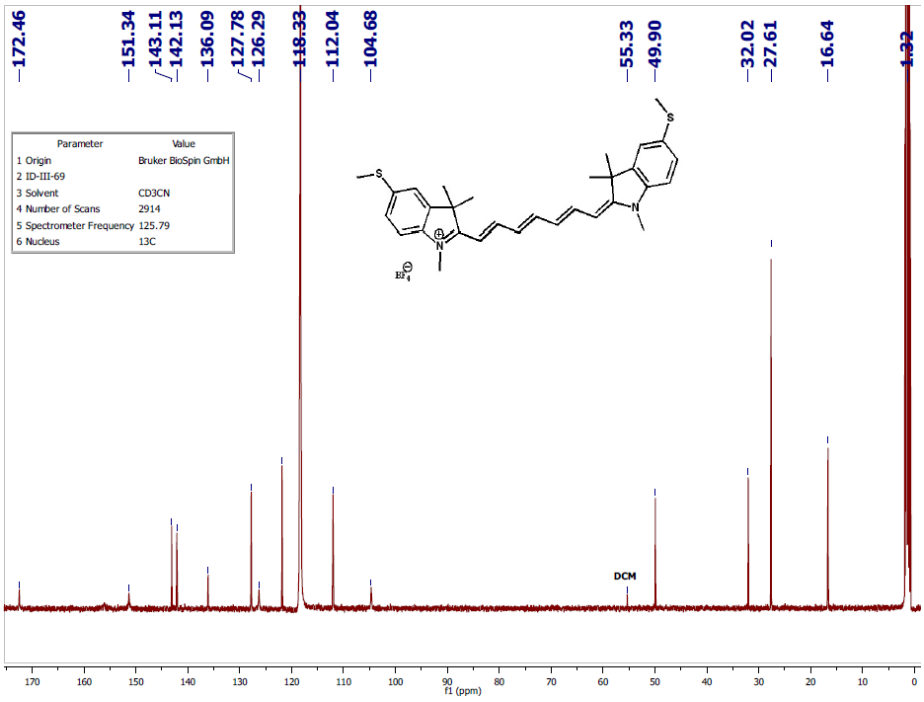

$^{13}C\{^{1}H\}$ NMR for compound **D3** in CD_3CN.

4. Additional Figures

a) Nonanol

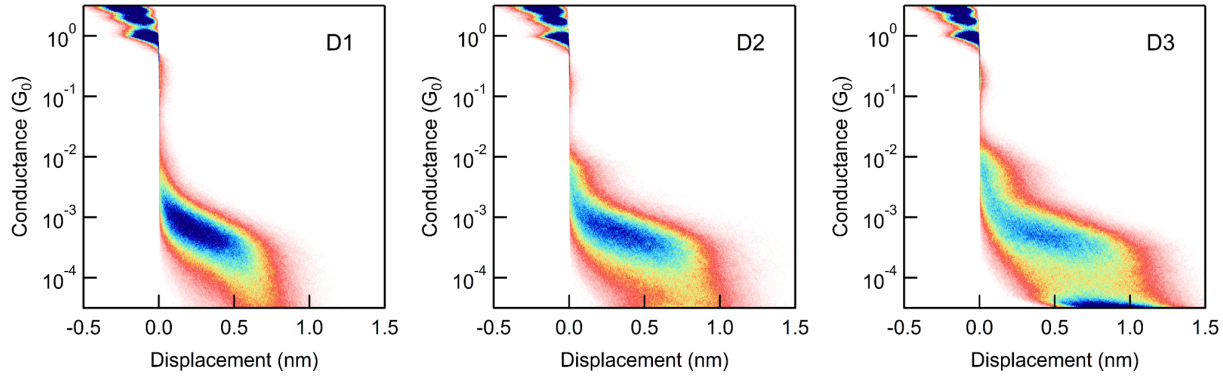

b) TCB

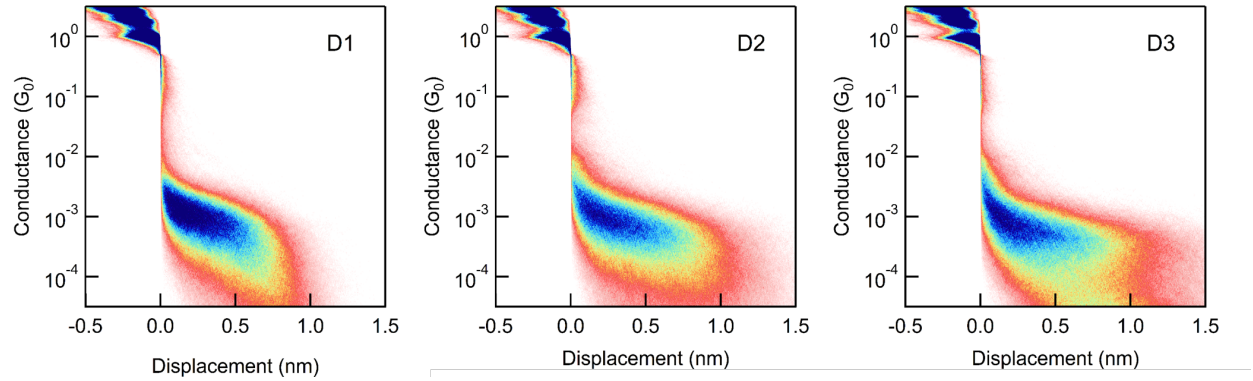

c) PC

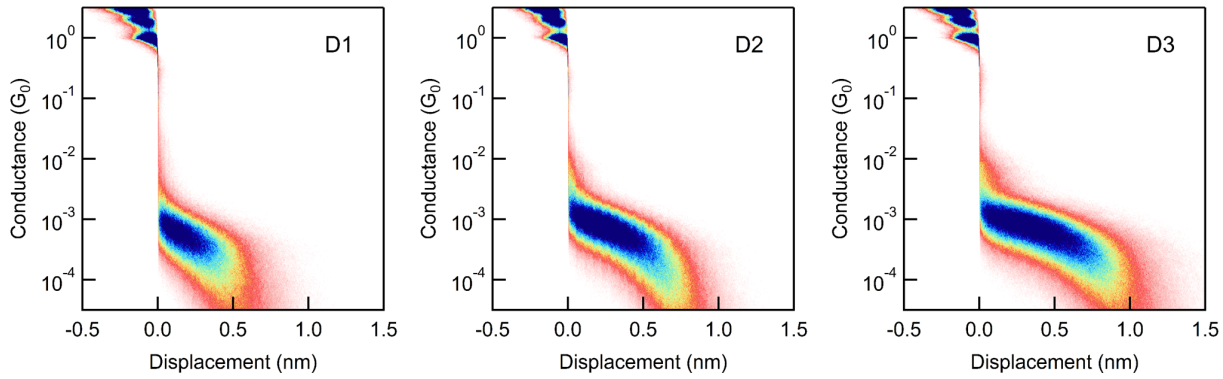

Figure S2. 2D Histograms for 0.1 mM **D1-D3** in (a) 1-nonanol, (b) TCB and (c) PC (10,000 traces each). While the conductance stays nearly constant in all three solvents, the maximum elongation increases with increasing molecular length from **D1** to **D3**.

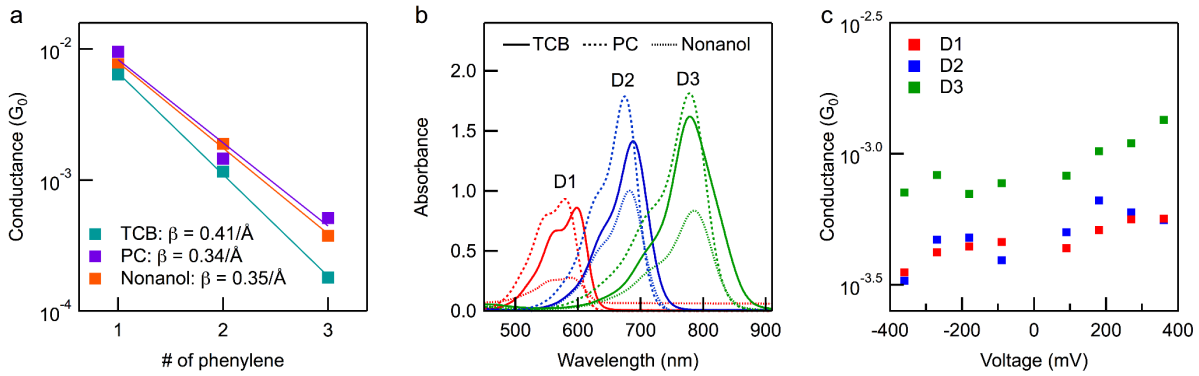

Figure S3. (a) Length-dependent conductance of oligophenylene diamines in 1-nonanol, TCB, and PC. The measured β values are roughly independent of solvent. **(b)** UV-Vis absorption spectrum for **D1-D3** in TCB, PC and 1-nonanol. Optical gaps determined from these data are (eV): **D1**: 1.96, 2.00, 1.97, **D2**: 1.66, 1.70, 1.69, **D3**: 1.42, 1.47, 1.46; for TCB, PC, and 1-nonanol, respectively. **(c)** Bias-dependent measurements of **D1-D3** in PC. Each data point represents the peak position of 4,000 conductance traces. The slight positive slope indicates that transport is off-resonance and that the molecules are HOMO conducting.[1]

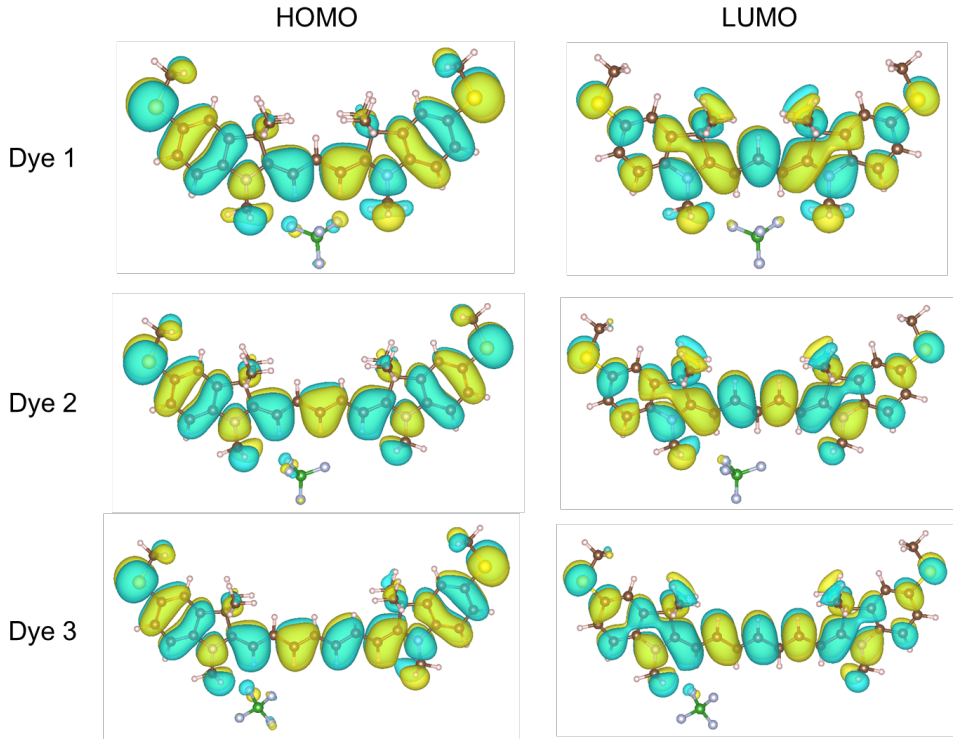

Figure S4. Isosurface plots of the HOMO and LUMO Kohn-Sham states for **D1-D3** isolated molecules.

5. Quantum Transport Calculations Details

We performed *ab-initio* quantum transport calculations based on the closed-shell Kohn-Sham formulation of density functional theory used in the FHI-aims package,[2] with a non-empirical generalized gradient-corrected (PBE) approximation for the exchange-correlation functional.[3] Scalar relativistic corrections to the kinetic energy of all atoms are taken into account within the zeroth-order regular approximation (ZORA).[4] The Kohn-Sham wavefunctions are represented in an optimized all-electron localized basis set ('tight' computational settings, roughly similar to 'double-zeta + polarization' quality for the molecular atoms and 'double-zeta' quality for the gold atoms belonging to the electrodes). The ground state was obtained using reliable convergence criteria in the self-consistent field cycle for the difference in the particle density (10^{-5}), total energy (10^{-6} eV) and forces (10^{-4} eV/Å).

The geometry of the model junctions used in the transport calculations is obtained using a two-stage process. In a first step, the positions of all the molecular and apex atoms (with pyramidal clusters containing up to 11 gold atoms) are optimized using an enhanced version of the Broyden-Fletcher-Shanno-Goldfarb optimization algorithm.[2] Structures were considered relaxed only when the components of the residual forces per atom dropped below the threshold value 10^{-2} eV/Å. In a second step, the molecular and tip geometries are fixed and additional layers of gold atoms are added to the external planes of the optimized electrodes to ensure the screening of the excess charge in the subsequent transport calculations.

The electronic transmission is calculated using the non-equilibrium Green's function formalism applied to finite clusters as implemented in the module AITRANSS.[4, 5] Each lead contains up to 37 atoms and is represented by two pyramidal face centered (111) clusters. The self-energy of the reservoirs is approximated by an energy-independent (Markovian) local function, $\Sigma_{L/R}(\mathbf{r},\mathbf{r}') = [\delta\epsilon(\mathbf{r}) + i\eta(\mathbf{r})]\delta(\mathbf{r}-\mathbf{r}')$, with non-zero values only in the "surface" subspace associated to the most external layers of the electrode. The local leakage function, $\eta(\mathbf{r})$, is adjusted to ensure that the transmission function is invariant under smooth moderate changes in $\eta(\mathbf{r})$. The additional compensating energy shifts, $\delta\epsilon(\mathbf{r})$, prevent the presence of spurious electric charge accumulation at the boundaries of the metallic cluster.

Finally, note that our DFT-based quantum transport calculations do not explicitly address the effect of different solvents on the molecular junction. However, as presented in the main text, they provide valuable insights into the general mechanisms at play in the manifestation of reduced

attenuation parameter in cyanine dyes and in the understanding of the effect of solvent polarity on the molecular junction transmission characteristics.

6. HOMO-LUMO Gap in Cyanine Dyes

We provide here for completeness the values of the HOMO-LUMO gap for the cyanine dyes **D1-D3** in the presence of a tetrafluoroborate anion (gas phase):

	HOMO-LUMO gap [eV]	
	PBE	**PBE0**
D1	1.47	2.74
D2	1.25	2.39
D3	1.15	2.23

7. Bond Length Alternation Details

We quantify the molecular bond length alternation (BLA) by using a *local* BLA measurement in the central polymethine chain considered in our Hückel model. This term is defined as,

$$\Sigma_i = \frac{l_{i+1} - l_i}{\frac{1}{2}(l_{i+1} + l_i)}$$

where l_i is the bond length between atoms $i+1$ and i. With this definition, the sign of Σ_i relates to whether the next bond is longer $(+)$ or shorter $(-)$ than the present one normalized to their average length. We next define an *absolute average* BLA $:= \langle|\Sigma_i|\rangle$ in which we consider only the absolute differences between lengths of nearest neighbor bonds.

For the cyanine dyes **D1-D3** attached to gold clusters, the calculated absolute average BLA are very small: $|\Sigma_{D1}| = 0.81\%$, $|\Sigma_{D2}| = 0.89\%$, $|\Sigma_{D3}| = 1.25\%$ (**Figure S5**). In addition, we observe that the local BLA is reduced in the region of the polymethine wire that is close to the anion and local alternation of bond lengths can be completely muted for the shortest dye, **D1**, as nearest neighbors bond orders become almost equal.

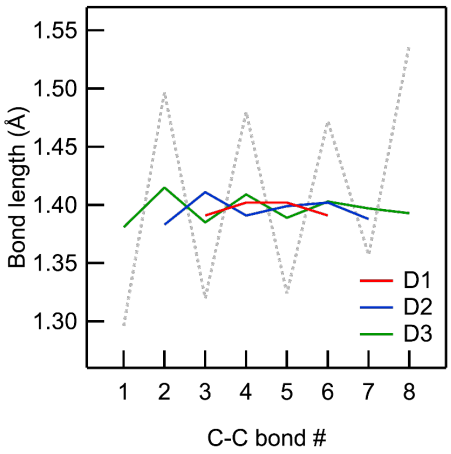

Figure S5. C-C bond lengths for **D1-D3** compared to a representative polyene (gray).[6] The BLA for **D1-D3** is significantly smaller than for polyene.

8. Derivation of *T(E)*

With the leads coupled to sites $|1\rangle$ and $|N\rangle$, we model the transmission function as[7]

$$T(E) = \Gamma_L \Gamma_R \left| G_{1,N} \right|^2, \tag{1}$$

where $G_{1,N}$ is the element $(1, N)$ of the Green's function, $G(E) = [EI - H_N]^{-1}$, with I the identity matrix. For $E_F = E_C = 0$, the Green's function simplifies to $G(E_F) = -H_N^{-1}$. By exploiting Cramer's rule, where $\Delta_{N,1}$ represents the minor determinant, we can then express the transmission at E_F as,

$$T(E_F) = \Gamma_L \Gamma_R \left| \frac{\Delta_{N,1}}{det(H_N)} \right|^2. \tag{2}$$

The determinant of H_N and the minor determinant can be calculated analytically:

$$\begin{aligned} \det(H_{2n}) &= (-1)^n \left(t_2^{2n} + t_1^{2(n-1)} \Gamma_L \Gamma_R / 4 \right) \text{ and } \Delta_{2n,1} = t_2^n t_1^{n-1} \\ \det(H_{2n+1}) &= (-1)^n \left(t_2^{2n} \frac{i}{2} \Gamma_R + t_1^{2n} \frac{i}{2} \Gamma_L \right) \text{ and } \Delta_{2n+1,1} = {t_2}^n {t_1}^n \end{aligned} \tag{3}$$

Thus, transmission at the Fermi energy is:

$$T(E_F) = \begin{cases} \left| \dfrac{2t_2^n t_1^{n-1}\sqrt{\Gamma_L\Gamma_R/4}}{t_2^{2n} + t_1^{2(n-1)}\Gamma_L\Gamma_R/4} \right|^2 & N = 2n \\ \left| \dfrac{2t_2^n t_1^n \sqrt{\Gamma_L\Gamma_R}}{t_2^{2n}\Gamma_R + t_1^{2n}\Gamma_L} \right|^2 & N = 2n+1 \end{cases} \tag{4}$$

These expressions can be re-written with the hyperbolic secant function to give Eq. 2. Transmission for cyanine, Eq. 4, is obtained by the substitution: $\frac{i}{2}\Gamma_{L(R)} \rightarrow \frac{i}{2}\Gamma - \varepsilon$ in Supplementary Eq. 3.

9. Derivation of β from Complex Band Structure

The dispersion relation for polyacetylene is given by[8],

$$E^2 = {t_1}^2 + {t_2}^2 + t_1 t_2\left(e^{i\kappa} + e^{-i\kappa}\right), \tag{5}$$

with $\kappa = k + i\beta/2$, in units of the lattice constant, and $E_F = 0$. The extended complex band structure[9] manifests as three regimes of solutions:

$$E = \begin{cases} \pm\sqrt{t_1^2 + {t_2}^2 + 2t_1 t_2 \cosh\beta/2} & \kappa = i\beta/2 \qquad |E| > |t_1 + t_2| \\ \pm\sqrt{t_1^2 + t_2^2 + 2t_1 t_2 \cos k} & \kappa = k \qquad |t_1 - t_2| < |E| < |t_1 + t_2| \\ \pm\sqrt{t_1^2 + t_2^2 - 2t_1 t_2 \cosh\beta/2} & \kappa = \pi + i\beta/2 \qquad |E| < |t_1 - t_2| \end{cases} \tag{6}$$

Within the band gap, $|E| < |t_1 - t_2|$, we derive the energy dependent β_∞,[10, 11]

$$\beta_\infty(E) = 2\cosh^{-1}\left(\frac{t_1^2 + t_2^2 - E^2}{2t_1 t_2}\right) \tag{7}$$

This simplifies at $E = E_F$ with $t_1 = t_0 e^{\delta}$ and $t_2 = t_0 e^{-\delta}$,

$$\beta_\infty(E_F) = 4|\delta|. \tag{8}$$

10. References

1. Capozzi, B.; Low, J. Z.; Xia, J. L.; Liu, Z. F.; Neaton, J. B.; Campos, L. M.; Venkataraman, L. *Nano Lett.,* **2016,** 16, (6), 3949-3954.
2. Blum, V.; Gehrke, R.; Hanke, F.; Havu, P.; Havu, V.; Ren, X.; Reuter, K.; Scheffler, M. *Comp. Phys. Commun.,* **2009,** 180, (11), 2175-2196.
3. Perdew, J. P.; Burke, K.; Ernzerhof, M. *Phys. Rev. Lett.,* **1996,** 77, (18), 3865-3868.
4. Vanlenthe, E.; Baerends, E. J.; Snijders, J. G. *J. Chem. Phys.,* **1994,** 101, (11), 9783-9792.
5. Arnold, A.; Weigend, F.; Evers, F. *J. Chem. Phys.,* **2007,** 126, (17), 174101.
6. Mechlinski, W.; Schaffner, C. P.; Ganis, P.; Avitabile, G. *Tetrahedron Lett.,* **1970**, (44), 3873-76.
7. Tsuji, Y.; Stuyver, T.; Gunasekaran, S.; Venkataraman, L. *J. Phys. Chem. C,* **2017,** 121, (27), 14451-14462.
8. Heeger, A. J.; Kivelson, S.; Schrieffer, J. R.; Su, W. P. *Rev. Mod. Phys.,* **1988,** 60, (3), 781-850.
9. Li, J.; Tomfohr, J. K.; Sankey, O. F. *Physica E-Low-Dimensional Systems & Nanostructures,* **2003,** 19, (1-2), 133-138.
10. Al-Backri, A.; Zolyomi, V.; Lambert, C. J. *J. Chem. Phys.,* **2014,** 140, (10).
11. Onipko, A. *Phys. Rev. B,* **1999,** 59, (15), 9995-10006.